Nanoscale Res Lett (2010) 5:308–314
DOI 10.1007/s11671-009-9481-9

NANO EXPRESS

Various Quantum- and Nano-Structures by III–V Droplet Epitaxy on GaAs Substrates

J. H. Lee · Zh. M. Wang · E. S. Kim · N. Y. Kim · S. H. Park · G. J. Salamo

Received: 23 September 2009 / Accepted: 28 October 2009 / Published online: 15 November 2009
© to the authors 2009

Abstract We report on various self-assembled In(Ga)As nanostructures by droplet epitaxy on GaAs substrates using molecular beam epitaxy. Depending on the growth condition and index of surfaces, various nanostructures can be fabricated: quantum dots (QDs), ring-like and holed-triangular nanostructures. At near room temperatures, by limiting surface diffusion of adatoms, the size of In droplets suitable for quantum confinement can be fabricated and thus InAs QDs are demonstrated on GaAs (100) surface. On the other hand, at relatively higher substrate temperatures, by enhancing the surface migrations of In adatoms, super lower density of InGaAs ring-shaped nanostructures can be fabricated on GaAs (100). Under an identical growth condition, holed-triangular InGaAs nanostructures can be fabricated on GaAs type-A surfaces, while ring-shaped nanostructures are formed on GaAs (100). The formation mechanism of various nanostructures can be understood in terms of intermixing, surface diffusion, and surface reconstruction.

Keywords Droplet epitaxy · Nanostructures · High-index GaAs · Atomic force microscope · Molecular beam epitaxy

J. H. Lee (✉) · E. S. Kim · N. Y. Kim · S. H. Park
Department of Electronic Engineering, Kwangwoon University, Nowon-gu Seoul 139-701, South Korea
e-mail: jihoonleenano@gmail.com

Zh. M. Wang (✉) · G. J. Salamo
Institute of Nanoscale Science and Engineering, University of Arkansas, Fayetteville, AR 72701, USA
e-mail: zmwang@uark.edu

Introduction

Owing to their unique optoelectronic, and physical properties, self-assembled semiconductor quantum- and nanostructures have been the focus of rigorous research efforts in basic physics [1–5] and solid-state devices. As an example, a number of device applications have been demonstrated, i.e., lasers, detectors, sensors, photovoltaic cells, light-emitting diodes, and solid-state quantum computation [6–14]. Among diverse self-assembly approaches droplet epitaxy (DE) offers advantages over the conventional Stransky–Krastnov (S–K) approach and thus a unique route to the fabrication of unforeseen nanostructures [15–32]. For instance, the lattice mismatch required in S–K approach is not essential in DE approach. In S–K, the lattice mismatch between hetero-systems induces the strain, which has to relax at a critical thickness depending on the amount of mismatch, which leads to the formation of three dimensional (3-D) self-assembled nanostructures [16]. Thus, S–K approach has been widely utilized with such material systems as InAs/GaAs, InP/GaP, and InSb/GaSb. However, in the case of material systems of small or no-lattice mismatch such as GaAs/AlAs or GaSb/AlSb, S–K cannot be adapted to fabricate 3-D nanostructures. In these cases, DE can be utilized to overcome the limitation [16, 28, 29]. Also because of the nature of the S–K growth mechanism, the position of nanostructures in S–K approach is randomly distributed and thus the control is somewhat limited when one solely relies on the S–K. In addition, DE offers higher degree of freedom in the control of size and density of nanostructures. Because the conversion process of liquid-phase metal particles into semiconductors, which is generally referred to "crystallization" or "arsenization," is not limited to the innate strain or the material system, there is much higher degree of freedom in the control of the size of

nanostructures [15–32]. Also in DE of certain cases, the metal particle formation and crystallization can be repeated and thus the density of nanostructures can be easily controlled in principle. On the other extreme hand, the optical study of nanostructures requires the fabrication of super low density of nanostructures or subsequent out-situ processes to focus on a singular nanostructure. DE approach can provide ultra low density of nanostructures to the degree of 10^5 or 10^6 cm^{-2}, which are several orders of magnitude lower density as compared to that of the conventional method. Furthermore, DE also can be used to fabricate unforeseen nanostructures owing to the flexibility of liquid-phase metal droplets, i.e., unique nanostructures such as quantum dot molecules and ensembles, transition between single and double quantum rings, low-density QDs, and nano-scale templates have been demonstrated [15–32].

In this article, we show various self-assembled nanostructures by DE approach on various indexes of GaAs surfaces using solid-source molecular beam epitaxy (MBE). Specifically, depending on the DE environment and the choice of index of surfaces, the resulting nanostructures range from InAs QDs and InGaAs ring-shaped nanostructures on GaAs (100) and InGaAs triangular-holed nanostructures on type-A GaAs surfaces. In droplets with the size range suitable for quantum confinement can be fabricated by limiting surface diffusion of adatoms at near room temperatures. Thus, using these droplets, InAs QDs are demonstrated on GaAs (100). Meanwhile super lower density of InGaAs ring-shaped nanostructures can be fabricated on the same index by enhancing the adatoms surface diffusion at comparatively higher temperatures. At a similar growth environment, depending on the choice of index of surfaces, triangular-holed InGaAs nanostructures can be fabricated on GaAs type-A surfaces. The size and density of nanostructures are discussed as a function of substrate temperature and of surface index. Empirical growth models that describe the fabrication mechanisms of various nanostructures by DE are suggested in comparison with the growth condition and indexes of surfaces. This study aids in understanding the formation of various nanostructures on GaAs surfaces by DE approach.

Experimental Details

In these experiments, various nanostructures were fabricated on GaAs substrates including (100) and type-A high indexes using solid-source molecular beam epitaxy (MBE). On a molybdenum sample holder, samples were side-by-side mounted using In soldering. Before introducing the samples into a growth chamber, they were pre-treated in a divided degas chamber at 350°C for an hour, which minimized water molecules and other contaminants. In order to calibrate the growth rates of molecular sources and monitor surface reconstructions, an in situ Reflection High Energy Electron Diffraction (RHEED) system was utilized. Native surface Ga oxide was thermally removed at 580°C for 10 min and subsequently a 1-μm thick GaAs homo-epitaxial buffer layer was laid down. The growth rate (G_{rate}) of GaAs was 0.85 monolayer per second (ML/s) under the As_4 flux of 6.4 μTorr at 600°C. With an in situ annealing of 10 min to equilibrate the surface matrix, the surface was ready for the further epitaxial growth. As the first step of In DE, the substrate temperature (T_{sub}) was modified to appropriate ones and the choice of T_{sub} was mainly dependent on the size and density requirements. For instance, to realize smaller size that is sufficient for quantum confinement and high density enough for applications, the T_{sub} for the samples in Fig. 2 was chosen to be in the range of 20–35°C. In order to realize the very low density, T_{sub} was selected to be 250, 350, and 450°C for the results in Fig. 3. In the meantime, for the samples in Fig. 4, the T_{sub} was fixed at 350°C and the index of the surface was varied to introduce the misfit into the formation of nanostructures. Regardless of the size and density, to prevent background As effects, droplets were formed by applying molecular beams of In under the chamber background below 3×10^{-9} Torr. Droplets form because the bonding energy of In adatoms is greater than that between adatoms and the surface atoms, which is based on the Volmer–Weber growth model [33]. For the samples in Fig. 2, a total amount of 3 ML was deposited on GaAs (100) at a G_{rate} of 0.08 ML/s. Similarly, for the samples in Fig. 3, a total amount of 1 ML was applied at a G_{rate} of 0.08 ML/s on GaAs (100) at corresponding substrate temperatures. For the samples in Fig. 4, the total amount of In deposition was fixed at 1 ML on the entire index of surfaces used and the G_{rate} was 0.05 ML/s. For the fabrication of nanostructures, In droplets were further treated with various fabrication processes depending on the type of nanostructures, which is generally referred to "crystallization" as liquid-phase metal droplets are converted to semiconductors. Generally, crystallization was immediately executed right after the formation of droplets to prevent Ostwald-ripening of droplets [34, 35] and samples were immediately taken out of the chamber after growth processes. Detailed crystallization procedures are discussed in "Results and discussion." Ex situ atomic force microscope (AFM) characterization was performed in air using tapping mode. The construction of 2D and 3D topographic images and the analysis of data was performed using WSxM software by processing original AFM data [36].

Results and Discussion

Figure 1 shows a schematic of the formation of various nanostructures by droplet epitaxy on various GaAs

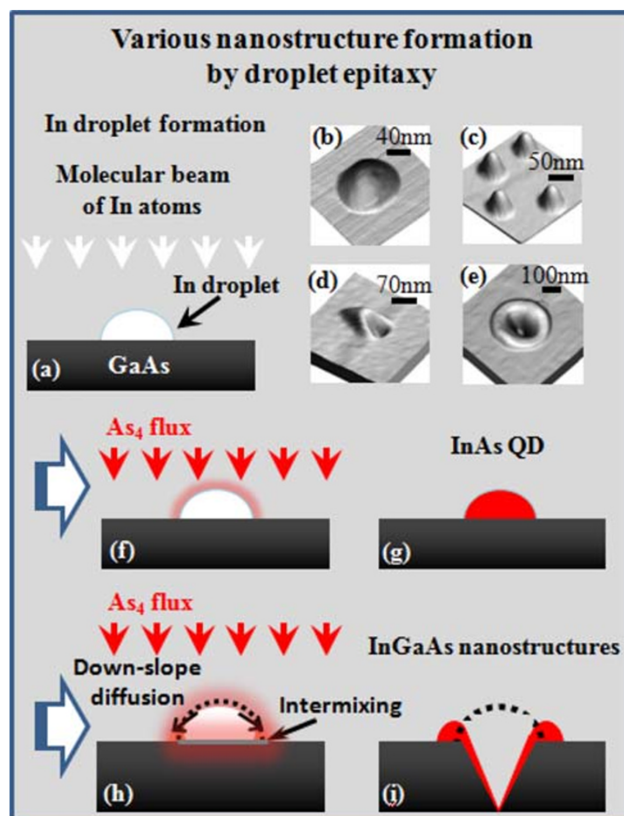

Fig. 1 Schematic of droplet epitaxy during the crystallization of In droplets into InAs and InGaAs nanostructures. From the formation of In droplet (**a**), the fabrication of InAs QDs (**c**) are described in (**f**, **g**). The fabrication schematic of various InGaAs nanostructures (**d**, **e**) at higher substrate temperatures are shown in (**h**, **i**)

surfaces. The formation of In droplets with an application of molecular beam of In atoms on GaAs surface is described in Fig. 1a and the actual In droplets fabricated at higher substrate temperature is shown in Fig. 1b as an example. From the droplet formation, they can be converted into InAs QDs through a crystallization process, which is described in Fig. 1f, g and the actual QDs are shown in Fig. 1c. Also depending on the crystallization condition and the index of surfaces, holed nanostructures can be fabricated, which is schematically described in Fig. 1h, i. As examples, triangular-holed nanostructures on GaAs type-A surfaces in Fig. 1d and ring-shaped nanostructures on GaAs (100) in Fig. 1e are shown.

Figure 2 shows the 2D and 3D atomic force microscopic (AFM) images of InAs QDs fabricated by DE at near room temperatures on GaAs (100) surface. The larger scale 2D AFM images are the areas of 1000 (x) × 700 (y) nm and insets of 3D images are 250 × 250 nm. These QDs were fabricated with 3-ML deposition at each substrate temperature of (a) 20, (b) 25, (c) 30, and (d) 35°C and followed by a subsequent crystallization process including exposing the droplets to an incoming As_4 flux (6.4 μTorr) for 5 min at each droplet formation temperature to recover the background pressure and enhancing the In and As interaction by heating the samples to 500°C [37]. The density of QDs was 5.4 × 10^{10} cm^{-2} at 20°C and 2.2 × 10^{10} cm^{-2} at 25°C. It was further decreased to 8.5 × 10^{9} cm^{-2} at 30°C and to 4.2 × 10^{9} cm^{-2} at 35°C. Given density at each temperature, the height and diameter of QDs were as follows: 40 nm (diameter: d) and 7.3 nm (height: h) at 20°C, 53.3 nm (d) and 10.2 nm (h) at 25°C, 66.7 nm (d) and 17.6 nm (h) at 30°C, and 90 nm (d) and 26.8 nm (h) at 35°C. Generally, as the substrate temperature was increased, the density of QDs was decreased and at the same time the diameter and height were increased. This can be explained with the surface diffusion of adatoms based on thermal dynamics of the epitaxial growth. That is the length of the surface migration of adatoms is strictly dependent on the T_{sub} and is increased at a higher temperature and vice versa. The longer the migration length of the adatoms, the lower the droplet density and the larger the droplet size can be expected. Thus, the size of droplets is greater at an increased T_{sub} and the density was reduced as the size and density should behave in an opposite way. In other words, in general, there is an inverse relationship between the density and size of droplet and thus the resulting QDs results in lower density at higher substrate temperature and vice versa for a fixed amount of deposition [17–20, 27–29]. One thing to notice in this set of samples is that the density of droplet was very sensitive to the temperature of 5°C as the surface migration of In adatoms is very sensitive to the T_{sub}. In terms of the growth mechanism, a simple scheme described in Fig. 1f, g can be used for InAs QDs as they are just converted from droplets into nano-crystalline semiconductors and the surface diffusion and the intermixing was kept at a minimum by a relatively low T_{sub} and background pressure recovery [37].

Figure 3 shows InGaAs ring-shaped nanostructures fabricated on GaAs (100) by DE at (a) 250, (b) 350, and (c) 450°C. The growth condition was similar to that used in samples in Fig. 2 except the T_{sub} for the deposition and crystallization of In droplets was much higher. The crystallization was right after the deposition of droplets, that is the As shutter was open immediately as the In shutter was closed. Now instead of QDs, InGaAs ring-shaped nanostructures were formed on the same index of substrate of GaAs (100). Based on the scheme of the surface diffusion of adatoms, the growths resulted in much smaller densities and the size of nanostructures was much larger. The density of InGaAs ring-shaped nanostructures was 7.4 × 10^{6} cm^{-2} at 250°C, 5.0 × 10^{6} cm^{-2} at 350°C, and 2.3 × 10^{6} cm^{-2} at 450°C, which is a few nanostructures per 10 × 10 μm and thus suitable for the study of single nanostructure spectroscopy [38]. The density of nanostructures in DE

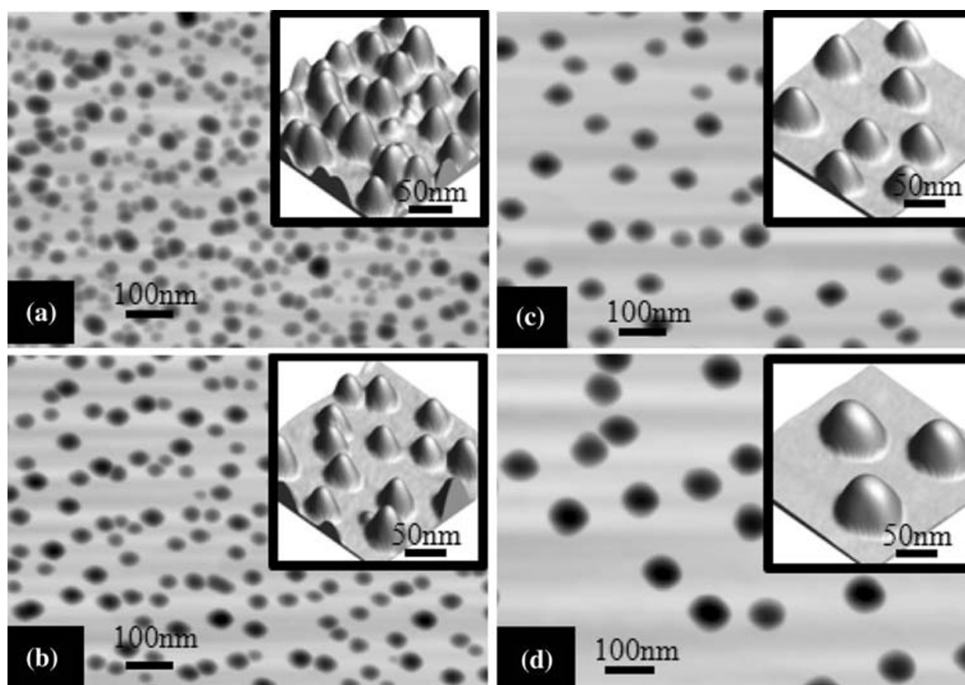

Fig. 2 2D and 3D atomic force microscope (AFM) images of InAs QDs on GaAs (100) surface at various fabrication temperatures: **a** 20, **b** 25, **c** 30, and **d** 35°C. Depending on the growth temperature, the size and density of QDs vary. The 2D AFM images are 1000 (x) × 700 (y) nm^2 and the 3D *insets* are 250 × 250 nm^2

normally tends to stay almost the same unless the surface diffusion becomes extremely severe or the initial size of droplets was small. Here the size of droplets was relatively large and they follow the general scheme of surface diffusion of adatoms, i.e., smaller size and higher density at lower T_{sub} and vice versa [17–20, 27–29]. As for the growth mechanism of holed InGaAs ring-shaped nanostructures, in simple, after the deposition of droplets at a higher T_{sub}, there is a severe surface intermixing at the boundary between droplets and substrate, resulting in the compound of In and Ga. This leads to the As desorption from the substrate and the As atoms diffuse out of the droplets as they are not allowed in the metal matrix according to phase diagram. Then, the In droplet further results in the melting of the GaAs surface and forms a hole down the substrate. Meanwhile, there is incoming As flux and thus this leads to the formation of InGaAs. Finally the diffusion was guided by the surface reconstruction of GaAs (100) surface. Therefore, the nanostructure resulted in a relative lower height along [01−1] because the surface diffusion is higher along this direction as the dangling bonds are reconstructed in a way that prefers the diffusion along the [01−1] direction [38].

Finally, Fig. 4 shows triangular-holed InGaAs nanostructures on InGaAs nanostructures on type-A GaAs surfaces: (311)A in Fig. 4a, (411)A in Fig. 4b, and (511)A in Fig. 4c. These nanostructures were fabricated under the similar growth condition of the samples in Fig. 3b. That is, the crystallization was immediately followed by the formation droplets at a fixed T_{sub}. Droplet formation and crystallization were at 350°C with 1 ML of In. First of all, while ring-shaped nanostructures were formed on GaAs (100), triangular-shape-holed nanostructures were formed on type-A GaAs surfaces. As clearly seen, the directionality of nanostructures and the direction of hole formation is uniform throughout the surfaces. In common as clearly seen in Fig. 4a–c, the formation of hole was along [2−n−n], where 'n' denotes the first index of surfaces. In addition, the density of nanostructures formed on GaAs (100) and type-A surfaces was quite very different even though the growth condition was identical. The density of InGaAs nanostructures was 8.2×10^7 cm^{-2} on (311)A, 4.7×10^7 on (411)A, and 1.1×10^7 on (511)A. In general, the density was one-order magnitude lower on GaAs (100) surface under an identical growth condition (7.4×10^6 cm^{-2} on (100)). Also within the type-A surfaces, there appeared a trend of gradual decreasing density with the increasing surface index at a fixed T_{sub}. This indicates that the size of droplets and thus the size of nanostructures were increased with the increasing surface index. This density variation depending on the surface indexes at a fixed T_{sub} can be attributed to the migration length of adatoms. In general, GaAs (100) is identified as a surface with no mis-cut along any directions. When a mis-cut is introduced along [01−1], this is known as type-B surfaces, while type-A surface is cut along [011]. The surface can be either predominantly Ga- or As-terminated. Generally the surfaces with a mis-cut less than 10° is referred to "vicinal," and when a

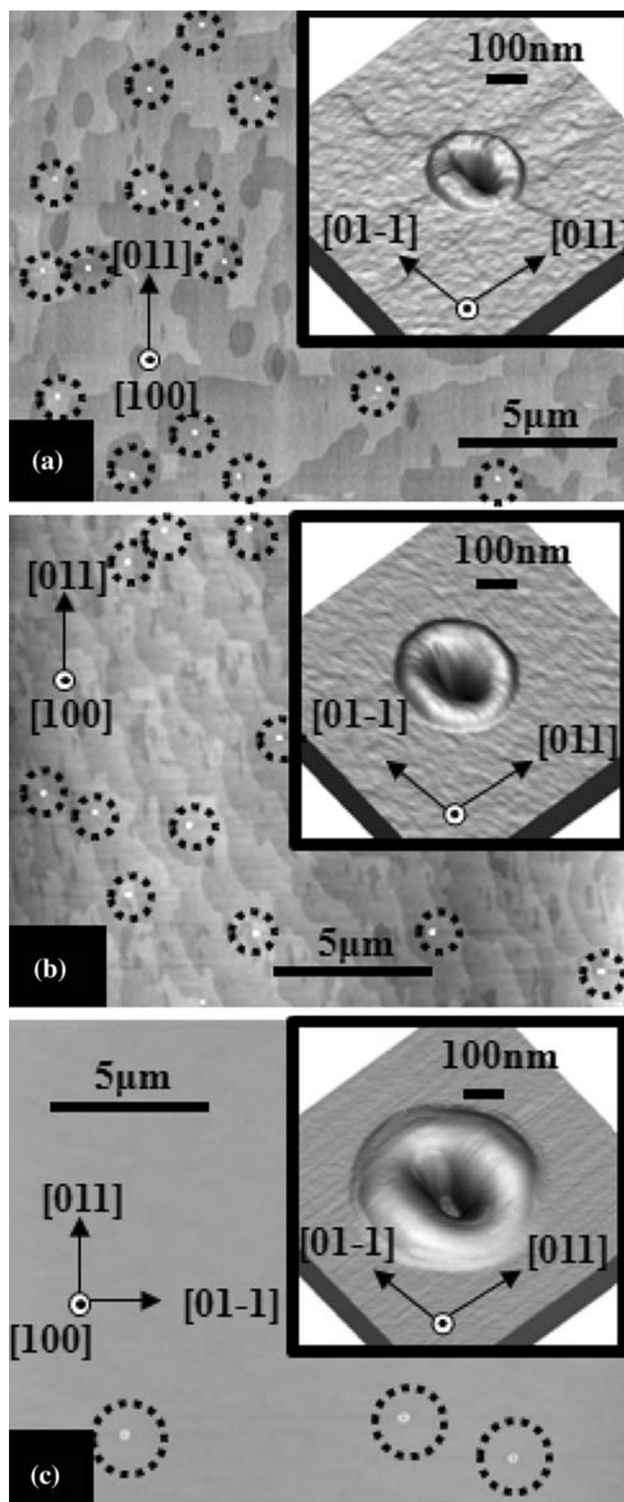

Fig. 3 2D and 3D AFM images of ring-shaped InGaAs nanostructures on GaAs (100) by droplet epitaxy: **a** 250, **b** 355, and **c** 450°C. Large 2D AFMs images are 20 (x) × 16 (y) μm^2 and the 3D *insets* are 600 × 600 nm^2. The *dotted-circle* emphasizes the location of nanostructures

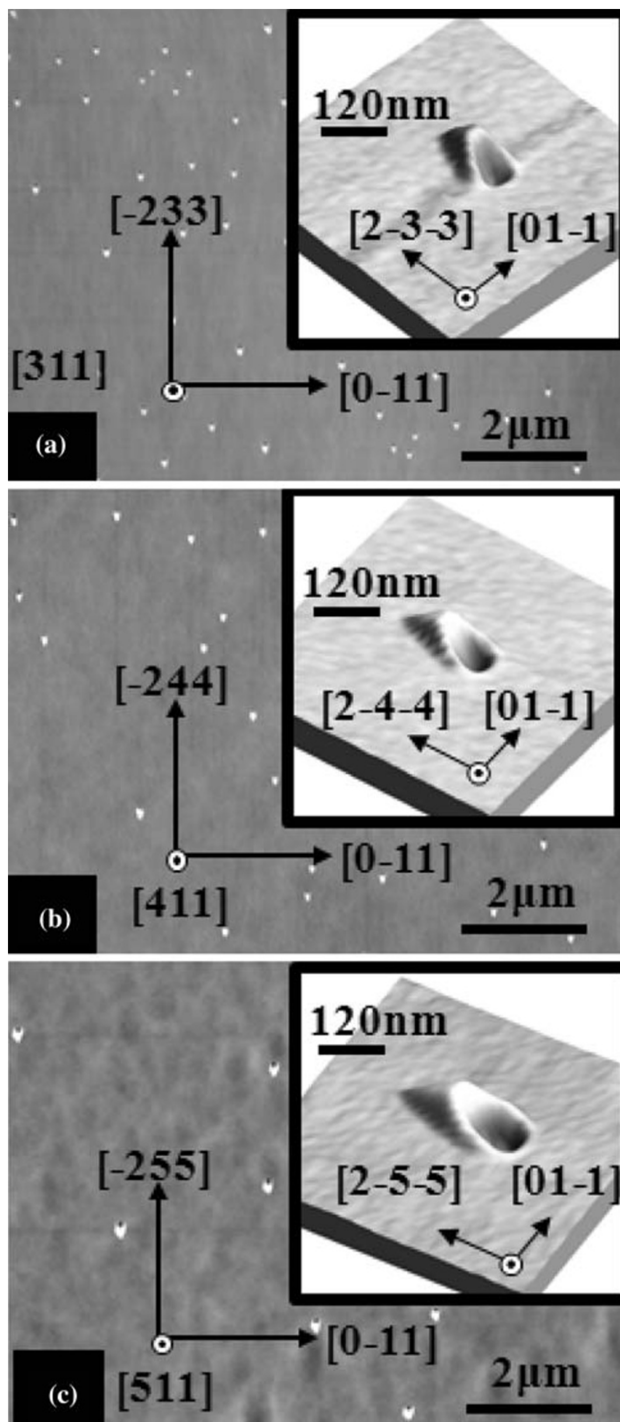

Fig. 4 2D and 3D AFM images of InGaAs triangular-holed nanostructures on GaAs type-A surfaces, which was fabricated at 350°C: **a** (311)A, **b** (411)A, and **c** (511)A. Large AFM images are 20 (x) × 16 (y) μm^2 and the 3D *insets* are 600 × 600 nm^2

greater mis-cut is introduced, this is known as a “high index” surface. For instance, GaAs (311)A surface has the miscut of 25.2° and (411)A is 19.5°, (511)A is 15.8° off toward [011]. The importance of mis-cut in the surface migration of adatoms is in that the probability of the length of the migration of adatoms is dependent on the density of the monolayer steps (MSD) of the surface [39, 40]. For example, GaAs (511)A has the MSD of 0.909 nm^{-1} with a step width (SW) of 1.1 nm. On GaAs (411)A the MSD is now increased to 1.25 nm^{-1} with the SW of 0.8 nm. Likewise, the MSD of 1.663 nm^{-1} on GaAs (311)A with the SW of 0.6 nm. This shows that the MSD increases with the increased mis-cut. Intuitively, with a higher MSD, a shorter diffusion length can be expected and thus this explains the density trend: higher density with lower index of surface [39, 40]. For the growth mechanism, an additional step can be introduced from the ring-shaped samples that explain the formation of holes and lobes. Now highly anisotropic surface diffusion can be introduced due to the atomic configuration of high-index surfaces, which is diamond symmetry along $[2{-}n{-}n]$ [40, 41]. Although there is an equal possibility of diffusion along $[2{-}n{-}n]$ and $[-2nn]$, because the dangling bonds are reconstructed along $[2{-}n{-}n]$, the nano-crystal matrix diffused toward $[2{-}n{-}n]$ as seen in Fig. 4.

Conclusions

The fabrication of various In(Ga)As nanostructures was demonstrated on various GaAs surfaces by droplet epitaxy using solid-source molecular beam epitaxy (MBE). At near room temperature, with the limitation of surface diffusion of adatoms, InAs QDs were demonstrated on GaAs (100). At higher surface temperatures, because of the enhanced surface diffusion, several orders of magnitude lower density of InGaAs nanostructures were demonstrated at the same surface. While ring-shaped GaAs nanostructures were formed on GaAs (100), triangular-holed InGaAs nanostructures were formed on GaAs type-A surfaces and the density and size was controlled by the selection of the surface index. The growth mechanisms of nanostructures were explained as follows: simple crystallization of In droplets into InAs nano-crystals in the case of QDs. For the ring-shaped and triangular-holed InGaAs nanostructures, the growths were the concurrent result of intermixing, dissolution of GaAs by In droplets and strong anisotropic surface diffusion guided by reconstructed surface matrix. This result can find applications in the formation of quantum- and/or nano-structures based on droplet epitaxy.

Acknowledgments The authors acknowledge the financial support of the NSF through Grant No. DMR-0520550 and the ONR through Grant No. N00014-00-1-0506. This research was partially supported by the MKE, Korea under the ITRC Support program supervised by the IITA (IITA-2009-C1090-0902-0018).

References

1. J. Tersoff, C. Teichert, M.G. Lagally, Phys. Rev. Lett. **76**, 1675 (1996)
2. S. Schmitt-Rink, D.A.B. Miller, D.S. Chemla, Phys. Rev. B **35**, 8113 (1987)
3. M. Grundmann, O. Stier, D. Bimberg, Phys. Rev. B **52**, 11969 (1995)
4. D.J. Mowbray, M.S. Skolnick, J. Phys. D **38**, 2059 (2005)
5. D. Stepanenko, G. Burkard, Phys. Rev. B **75**, 085324 (2007)
6. D.P. DiVincenzo, Science **309**, 2173 (2005)
7. G. Burkard, D. Loss, D.P. DiVincenzo, Phys. Rev. B **59**, 2070 (1999)
8. A. Imamoglu, D.D. Awschalom, G. Burkard, D.P. DiVincenzo, D. Loss, M. Sherwin, A. Small, Phys. Rev. Lett. **83**, 4204 (1999)
9. X. Xu, D.A. Williams, J.R.A. Cleaver, Appl. Phys. Lett. **86**, 012103 (2005)
10. Y.M. Kim, K.H. Hong, B.H. Lee, 3D Res. **1**, 010102 (2009)
11. X. Li, Y. Wu, T.H. Stievater, D.G. Steel, D. Gammon, D.S. Katzer, D. Park, C. Piermarocchi, L. Sham, Science **301**, 809 (2003)
12. T. Unold, K. Mueller, C. Lienau, T. Elsaesser, A.D. Wieck, Phys. Rev. Lett. **94**, 137404 (2005)
13. F. Troiani, U. Hohenester, E. Molinari, Phys. Rev. B **62**, R2263 (2000)
14. S.-S. Li, G.-L. Long, F.-S. Baii, S.-L. Feng, H.-Z. Zheng, Proc. Natl Acad. Sci. **98**, 11847 (2001)
15. T. Mano, T. Kuroda, S. Sanguinetti, T. Ochiai, T. Tateno, J. Kim, T. Noda, M. Kawabe, K. Sakoda, G. Kido, N. Koguchi, Nano Lett. **5**, 425 (2005)
16. I.N. Stranski, L. Krastanov, Zur theorie der orientierten ausscheidung von ionenkristallen aufeinander. Sitzungsber. Akad. Wiss. Wien. Math.-Naturwiss. **146**, 797–810 (1938)
17. J.H. Lee, Zh.M. Wang, N.W. Strom, Yu.I. Mazur, G.J. Salamo, Appl. Phys. Lett. **89**, 202101 (2006)
18. J.H. Lee, Z.M. Wang, B.L. Liang, K.A. Sablon, N.W. Strom, G.J. Salamo, Semicond. Sci. Technol. **21**, 1547 (2006)
19. Zh.M. Wang, B.L. Liang, K.A. Sablon, G.J. Salamo, Appl. Phys. Lett. **90**, 113120 (2007)
20. J.H. Lee, Z.M. Wang, S. Kim, G.J. Salamo, Cryst. Growth Des. **8**, 690 (2008)
21. Z. Gong, Z.C. Niu, S.S. Huang, Z.D. Fang, B.Q. Sun, J.B. Xia, Appl. Phys. Lett. **87**, 093116 (2005)
22. M. Yamagiwa, T. Mano, T. Kuroda, T. Tateno, K. Sakoda, G. Kido, N. Koguchi, F. Minami, Appl. Phys. Lett. **89**, 113115 (2006)
23. K.A. Sablon, J.H. Lee, Zh.M. Wang, J.H. Shultz, G.J. Salamo, Appl. Phys. Lett. **92**, 203106 (2008)
24. K.A. Sablon, Zh.M. Wang, G.J. Salamo, Nanotechnology **19**, 125609 (2008)
25. Ch. Heyn, A. Stemmann, A. Schramm, H. Welsch, W. Hansen, A. Nemcsics, Phys. Rev. B **76**, 075317 (2007)
26. N. Pankaow, S. Panyakeow, S. Ratanathammaphan, J. Cryst. Growth **311**(7), 1832 (2008)
27. J.H. Lee, Z.M. Wang, Z.Y. Abuwaar, N.W. Strom, G.J. Salamo, Nanotechnology **17**, 3973 (2006)
28. B.L. Liang, Zh.M. Wang, J.H. Lee, K. Sablon, Yu.I. Mazur, G.J. Salamo, Appl. Phys. Lett. **89**, 043113 (2006)
29. B.L. Liang, Zh.M. Wang, J.H. Lee, K.A. Sablon, Yu.I. Mazur, G.J. Salamo, Appl. Phys. Lett. **89**, 213103 (2006)

30. C. Zhao, Y.H. Chen, B. Xu, C.G. Tang, Z.G. Wang, F. Ding, Appl. Phys. Lett. **92**, 063122 (2008)
31. C.Z. Tong, S.F. Yoon, Nanotechnology **19**, 365604 (2008)
32. A. Stemmann, Ch. Heyn, T. Köppen, T. Kipp, W. Hansen, Appl. Phys. Lett. **93**, 123108 (2008)
33. M. Volmer, A. Weber, Z. Phys. Chem. **119**, 277 (1926)
34. B.D. Min, Y. Kim, E.K. Kim, S.-K. Min, M.J. Park, Phys. Rev. B **57**, 11879 (1998)
35. S. Lee, I. Daruka, C.S. Kim, A.-L. Barabási, J.L. Merz, J.K. Furdyna, Phys. Rev. Lett. **81**, 3479 (1998)
36. I. Horcas, R. Fernández, J.M. Gómez-Rodríguez, J. Colchero, J. Gómez-Herrero, A.M. Baro, Rev. Sci. Instrum. **78**, 013705 (2007)
37. J.H. Lee, Z.M. Wang, G.J. Salamo, IEEE Trans Nanotechnol **8**, 431 (2009)
38. J.H. Lee, Z.M. Wang, M.E. Ware, K.C. Wijesundara, M. Garrido, E.A. Stinaff, G.J. Salamo, Cryst. Growth Des. **8**, 1945 (2008)
39. Zh.M. Wang, Sh. Seydmohamadi, J.H. Lee, G.J. Salamo, Appl. Phys. Lett. **85**, 5031 (2004)
40. J.H. Lee, Z.M. Wang, Z.Y. AbuWaar, G.J. Salamo, Cryst. Growth Des. **9**, 715 (2009)
41. L. Geelhaar, J. Márquez, K. Jacobi, Phys. Rev. B **60**, 15890 (1999)